3D-VISUALIZATION OF INTERFEROMETRIC SAR DATA

U. Sörgel, K. Schulz, U. Thönnessen, U. Stilla

FGAN-FOM Forschungsinstitut für Optronik und Mustererkennung
Gutleuthausstraße 1, D-76275 Ettlingen, Germany
Tel: +49-7243-992293, Fax: +49-7243-992299, E-mail: [soe,schulz,thoe,usti]@fom.fgan.de

ABSTRACT

The reliability of the interpretation of remotely sensed data can be increased by an appropriate 3D-visualization of the data. In this paper we refer to investigations which may stabilize and improve the visualization of InSAR height information. The height data is improved by a combined exploitation of intensity and height information using a model based segmentation process.

1 INTRODUCTION

Photo interpretation of remotely sensed data can be supported by appropriate visualization of the data, for example by mapping the imagery on a 3D-model of urban areas. A coarse 3D-description using prismatic models can be derived by masking the elevation data with co-registered vector maps, as shown in the literature using range information of laser systems [1].

Due to the improved quality and ground resolution of interferometric SAR data it is reasonable to use the available height information for this purpose in the future. But, in the case of SAR interferometric data many additional problems have to be taken into account, e.g. radiometric correction, layover effects, multi backscattering, speckle, phase unwrapping errors, relations and dependencies of intensity and noise in the height information. One advantage of SAR and InSAR data is, that these are co-registered. For a visualization mentioned before referencing of intensity and height information is not necessary. Unfortunately, especially the interferometric phase information suffers from noise. Furthermore, even small errors in the phase lead to big errors in the height values. Thus, the phase information has to be prepared for further processing. Smoothing of the height data, like phase multilook processing [2], blurs edges of man-made objects (e.g. building walls) and as a consequence, details may be lost. On the other hand, object borders can often be extracted in the intensity data because of the different backscattering behavior of different materials. Additionally, in many cases areas with comparatively homogeneous intensity distributions correspond to regions, respectively objects, with equal height information. Such regions are extractable by edge preserving region oriented image processing algorithms. In our approach we segment regions with similar intensity values in the speckle filtered intensity data using an edge sensitive region growing algorithm [3].

Segments with low mean intensity are masked, because low intensity is correlated with poor coherence.

Small regions are masked, too. In our test site, we are interested in man-made objects with constant height present in the scene like flat-roofed buildings. Hence, the height of one segmented object is set to the mean height over the segment, weighted with the intensity values.

2 INTERFEROMETRIC PRINCIPLE

Object of this paper are interferograms derived from airborne single pass measurements. Figure 1 illustrates the basic principle of SAR interferometry. An airplane carries two SAR antennas which are displaced by a baseline *B*. One of the antennas illuminates the scene and both antennas receive the backscattered complex signals s_1 and s_2.

The interferogram *S* is calculated by a pixel by pixel complex multiplication of the two received signals:

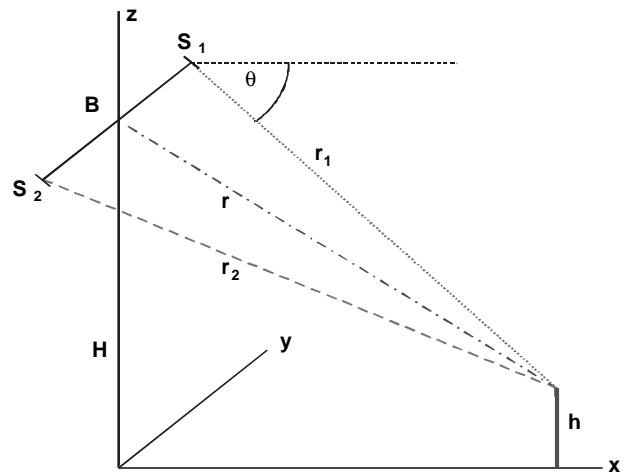$$S = |s_1| \cdot |s_2| \cdot \exp(j\Delta\varphi) \qquad (1)$$

Figure 1*: Geometry of InSAR Measurement*

The object height *h* can be expressed as a function of the phase difference *Δφ*:

$$h = \frac{\lambda \cdot r \cdot \cos(\theta)}{2\pi \cdot B} \cdot \Delta\varphi \qquad (2)$$

with parameters distance *r*, wavelength λ, effective baseline *B* and depression angle θ.

SAR interferometry makes only sense in case of significant correlation respectively coherence between the

two complex SAR images. The coherence γ depends on the expectation values of the signals. It can be estimated from the data by window-based computation of the magnitude $\hat{\gamma}$ of the complex cross-correlation coefficient of the SAR images [4] :

$$\hat{\gamma} = \frac{\left| \sum_{n=1}^{N} s_1^{(n)} \cdot s_2^{(n)*} \right|}{\sqrt{\sum_{n=1}^{N} \left| s_1^{(n)} \right|^2 \cdot \sum_{n=1}^{N} \left| s_2^{(n)} \right|^2}} \qquad (3)$$

In case of a single pass airborne system temporal and geometrical contributions to the coherence coefficient can be neglected compared to the influence of noise. Assuming additive thermal noise, the complex signals s_i can be modeled as consisting of a correlation part c and noise part n_i:

$$s_i = c + n_i \qquad (4)$$

The absolute value of γ can be expressed [7] as a function of the signal to noise ratio (SNR):

$$|\gamma| = \frac{1}{1 + \dfrac{1}{SNR}}, \quad with \quad SNR = \frac{|c|^2}{|n|^2} \qquad (5)$$

If no phase unwrapping errors occur, the standard deviation σ_h of the height measurement is:

$$\sigma_h = \frac{\lambda \cdot r}{2\pi \cdot B \cdot \sqrt{SNR}} \qquad (6)$$

Thus, the height accuracy declines with decreasing *SNR.*.

3 APPROACH

Smoothing directly in the height data without regarding the intensities reduces σ_h, but blurs height jumps in the scene like building walls.

Due to the interferogram calculation (equation 1) the height and intensity data are perfectly co-registered. Therefore, an exploitation of height and intensity data in combination is immediately possible. Concerning a model-based segmentation of man-made objects we propose as a first approach that regions with similar intensity values correspond to regions with equal height information. The regions are segmented in the intensity data with an edge sensitive region growing algorithm. Because of the additive noise model in equation 4 we consider segments with low intensity values as noisy and brighter areas as more reliable regions with higher *SNR*. Thus, segments with too small mean intensities are masked. Inside each remaining segment the weighted mean height is calculated, using the intensity values as weights.

Before the segmentation step the data has to be prepared by speckle filtering to avoid an "over-segmented" result.

3.1 PREPROCESSING

To limit the number of segments in the following region growing step, the intensity data has to be filtered to reduce the speckle effect. We tested several filters described in the literature. Best results for our purposes were achieved using a median and the ESTEC [5] filter. After despeckling the intensities are linear spread from 0 to 255 to achieve identical start configurations in the region growing step for different images.

In the filtered image the gradient is calculated. Pixel with a gradient higher than a threshold are considered as possible region borders. The threshold th_b is calculated from the average intensity (*mean*) and standard deviation *sd* of the entire intensity image:

$$th_b = mean + 2 \cdot sd \qquad (7)$$

The border candidate pixel are skeletonized by morphological operations [8][9]. The result is a binary image with thin borders.

3.2 SEGMENTATION

The edge sensitive region growing algorithm is fed with the speckle filtered scaled image and the binary border image. For a detailed description of the algorithm the reader is referred to [3].

Our goal is only to derive a coarse prismatic 3D-model. Therefore, we are not interested in small details like chimneys. To extract extended regions the maximal gray level distance threshold th_r for a pixel to the *mean* of a adjacent region has to be set to a high value. To prevent the algorithm to "bleed" over the entire image, which is a danger because of the high threshold, it was not allowed to cross the borders extracted before.

Small areas were masked as well as areas with low coherence, which are identified by mean intensity values below a threshold th_i:

$$th_i = mean - sd \qquad (8)$$

3.3 SMOOTHING OF THE HEIGHT DATA

Inside the remaining segments the height h_s of the segment with a number of N pixels is calculated by the mean of the heights h weighted with the intensity i:

$$h_s = \frac{\sum_{n=1}^{N} i^{(n)} \cdot h^{(n)}}{\sum_{n=1}^{N} i^{(n)}} \qquad (9)$$

Holes inside the weighted heights which result from the masking step are set to the height value of the surrounding region. The strategy towards the remaining holes depends on the task. Because of their unreliable information they should not be considered for further processing. However, for visualization purposes it is often better to set them to a default height, because holes in the evaluated depth map might irritate an interpreter.

4 RESULTS

The test data set consists of intensity and height images (Fig 2 a,b) of the Frankfurt (Main) airport area plus collateral data containing data acquisition and InSAR processing information. The airborne single pass ground range data has a resolution of 1m × 1m. A Transall airplane carried the sensor in approximately 3km flight height above the ground. The sensor operated in X-band with wavelength $\lambda = 3$cm, effective baseline $B = 1$m and depression angle $\theta = 43°$.

According to equation 2 this sensor configuration results in an unambiguous (phase difference $\Delta\varphi < 2\pi$) height range of approximately 100m in mid swath. Therefore, no phase ambiguities had to be taken into account to calculate the height from the phase information, in the comparatively flat scene with about 30m height difference.

A maximum *SNR* value of 100 (20 dB) is assumed in areas with high intensities in the interferogram. The lowest value for σ_h achievable is about 2.1m according to equation 6.

The depth map in figure 2c illustrates the result of the segmentation and weighting process. The gray values of the segmented regions correspond to the averaged height. For better visualization are the boundaries of the extended regions overlaid on the depth map. Compared to the original height data in Figure 2b the smoothed and averaged heights are more appropriate for visual interpretation. The detected unreliable segments, like the airfield traffic net, were not masked for the visualization. Their height was set to the average of all unreliable segments.

Problems occurred when objects with different height levels but similar backscatter behavior could not be separated in the segmentation step. In the question-mark-shaped large building in the lower right for example only two segments could be extracted. The height jumps between the levels were small and no edges between them could be detected in the intensity data. So, the different height levels were set to their weighted average in the two segments.

For better visualization and further interpretation the intensity values are mapped on a DEM derived from the calculated depth map (Figure 2d).

5 CONCLUSION AND FUTURE WORK

The approach of improving the interpretation of InSAR height information, using a model based segmentation process in the intensity data, achieved promising first results. The object model will be expanded to sloped objects (e.g. gable roofs) incorporating gradient based segmentation methods.

To overcome under-segmentation, like the one described in the previous chapter, the heights in the segments extracted in the intensity data could be segmented themselves. If different height levels can be found the segment is split up.

Our goal in the future will be to extract prominent edges in the image, to fuse this result together with the height information and to reconstruct man-made objects like buildings. The assumption for this step is the geometric and radiometric [8] correction of the SAR intensity image by the elevation model derived from the height image.

The segmented regions could be incorporated in the phase unwrapping step. Shadow and layover areas, which correspond to high intensity and low coherence, could be masked. Only residues in the remaining data are considered.

6 ACKNOWLEDGMENT

7 REFERENCES

[1] U. Stilla and K. Jurkiewicz: "Reconstruction of Building Models from Maps and Laser Altimeter Data", In: P. Agouris and A. Stefanidis (eds.) Integrated Spatial databases: Digital Images and GIS, Berlin Springer, 1999, pp. 39-46.

[2] R. Goldstein, H. Zebker and C. Werner: "Satellite Radar Interferometry: Two Dimensional Phase Unwrapping", Radio Science, Vol. 23, No. 4, 1988, pp. 713-720.

[3] M.D. Levine and S.I. Shaheen: "A modular Computer vision system for picture segmentation and interpretation", IEEE Trans. PAMI, Vol. PAMI-3 (5), September 1981, pp. 540-554.

[4] O. Hellwich: "Basic Principles and Current Issues of SAR Interferometry", ISPRS Joint Workshop: Sensors and Mapping from Space 1999, No. 18, Hannover.

[5] Y.-L. Desnos and V. Matteini: "Review on Structure Detection and Speckle Filtering on ERS-1 Images", EARSeL Advances in Remote Sensing, vol. 2, no. 2, Paris, 1993, pp. 52-65.

[6] J.H.G. Ender: "Experimental results achieved with the airborne multi-channel SAR system AER-II", Proc. EUSAR'98, 25-27 May, Friedrichshafen, Germany, pp. 315-318

[7] E. Rodriguez and J.M. Martin: "Theory and design of Interferometric Synthetic Aperture Radar", IEEE Proceedings-F, Vol. 139, No.2, pp.147-159.

[8] F. Glazer: "Morphological Image Processing in the KBVision System", Amerinex Artificial Intelligence, Inc., Technical Report, 1993.

[9] K. Schulz and U. Thönnesen: "Segmentation of Detail Structures of Extended Objects in SAR Images", 23-25 May, Munich, Germany, This issue.

[10] L.M.H. Ulander and J.O. Hagberg: "Use of InSAR for Radiometric Calibration over Sloping Terrain", Proc. of CEOS SAR Workshop, Noorwijk, 1993, pp. 147-159.

[11] R. Bamler and P. Hartl: "Synthetic Aperture Radar Interferometry", Inverse Problems 14(4), 1998, pp. 1-54.

a) Intensity Image	b) Height Image

c) Depth Map	d) 3D-Visualization

Figure 2: *3D-Visualization of Interferometric SAR Data*